IEEE Access
Multidisciplinary : Rapid Review : Open Access Journal

Received November 27, 2018, accepted December 8, 2018, date of publication January 10, 2019, date of current version January 23, 2019.

Digital Object Identifier 10.1109/ACCESS.2018.2889964

A New Chaotic Oscillator–Properties, Analog Implementation, and Secure Communication Application

CHRISTIAN NWACHIOMA[1,2], (Member, IEEE), J. HUMBERTO PÉREZ-CRUZ[2], ABIMAEL JIMÉNEZ[3], MARTINS EZUMA[4], (Member, IEEE), AND R. RIVERA-BLAS[2]

[1]CIDETEC, Instituto Politécnico Nacional, UPALM, Mexico 07700, Mexico
[2]ESIME-Azcapotzalco, Instituto Politécnico Nacional, Mexico 02250, Mexico
[3]Electrical and Computer Engineering Department, Universidad Autónoma de Ciudad Juárez, Ciudad Juárez, 32310, Mexico
[4]MPACT Lab, Department of Electrical Engineering, North Carolina State University, Raleigh, NC 27695, USA

Corresponding authors: Christian Nwachioma (christian.nwachioma@ieee.org) and Abimael Jiménez (abimael.jimenez@uacj.mx)

This work was supported by Secretaría de Investigación y Posgrados, Instituto Politécnico Nacional under Grant 20180054.

ABSTRACT This paper reports a new 3-dimensional autonomous chaotic system with four nonlinearities. The system is studied with respect to its numerical solutions in phase space, including sensitive dependence on initial conditions, equilibrium points, bifurcation, and maximal Lyapunov exponent. It is shown that the system is dissipative and has a fractional Lyapunov dimension. Besides, a basin of attraction is determined by the Newton–Raphson's method. To show its practicality, the new system is implemented by means of an analog electronic circuit. Aperiodicity of the experimental signal is verified by means of an improved power spectral density estimator, viz., the Welch's method. Also, the correlation dimension is estimated from the experimental time series with the result confirming that the responses are deterministic chaos. Finally, an electronic design of a secure communication application is carried out, wherein a nontrivial square wave is modulated by a *master* chaotic signal. The modulated signal is subsequently recovered by a *slave* system, and the fast convergence to zero of the information recovery error substantiates the effectiveness of the design.

INDEX TERMS Chaotic system, Lyapunov spectrum, bifurcation analysis, analog circuit, secure communication, self-synchronization.

I. INTRODUCTION

There has been a surge of research interests in chaos theory for over four decades. This is primarily due to its potential benefits across disciplines [1]–[11]. With chaos control [12]–[17], the window of applicability of chaos has widened. In the field of communication engineering for instance, chaos theory has been used in several communication techniques [18]–[25] including security of information [26]. Besides, the understanding of chaotic time series has shone more lights in the study of real world complex systems [27]. Moreover, other notable areas to which chaos theory has been applied include biological systems [28], [29], chemical systems [30], [31], nuclear reactor systems [32], economic [33] and political [34] systems, ecology [35], neural networks [36], [37], experimental data analysis [38] and so on.

This paper aims to report a new 3-dimensional autonomous chaotic system. Some novel qualities of the system include:

1) basic transformations on the system such as rotation or reflection can result in different algebraic systems, which are however, topologically equivalent to the original system.
2) the term $a_8x_1^2x_2$, which is very vital to the chaotic system since without it, the system becomes unbounded as simulation shows.
3) easy and robust analog implementation cf. [39]. This is a good requirement for engineering applications.
4) proper retention of chaotic feature when the system's signal is used to modulate digital signals.
5) having two nearly counteracting parameters, which can be varied in opposite sense to have nearly opposite effects on the attractor.

Due to some of these qualities, the system is easily implementable using analog electronic devices. Also, an electronic circuit design of a secure chaos-based digital signal transmission has been realized. To the best of our knowledge, there are very limited electronic circuit realization of chaos-based secure communication in the literature.

By the classification scheme in [40], the Lü system [41] satisfies $a_{12}a_{21} = 0$, $(a_{12} \neq 0, a_{21} = 0)$. The present system like the recently reported Zhou system [42] also satisfies $a_{12}a_{21} = 0$, $(a_{12} = 0, a_{21} = 0)$. These systems reside at the intersection between the Lorenz-like and the Chen-like systems which respectively satisfy $a_{12}a_{21} > 0$ and $a_{12}a_{21} < 0$. The present system has in addition to the linear and nonlinear terms, the constant terms unlike the Lü's and the Zhou's. Moreover, all three systems in the first classification have unequal numbers of equilibrium points. Hence, they are distinct [43].

II. SYSTEM DESCRIPTION

The new chaotic system is given by

$$\begin{aligned} \dot{x}_1 &= a_1x_1 + a_2x_1x_3 + a_3x_2x_3 \\ \dot{x}_2 &= a_4x_2 + a_5x_1x_3 + a_6 \\ \dot{x}_3 &= a_7x_3 + a_8x_1^2x_2 + a_9. \end{aligned} \tag{1}$$

Let $\boldsymbol{x} := \{x_i | i = 1, 2, 3\}$ be a state vector of the system. $a_k (k = 1, 2, .., 9)$ are constant parameters. By probing the parameter space [44] of system (1) by means of a computer search [45] for a region where the system possesses a positive Lyapunov exponent while remaining numerically bounded, it can be established that this system presents a chaotic regime for the following values: $a_1 = -0.1$, $a_2 = 0.15$, $a_3 = 0.18$, $a_4 = 3.9$, $a_5 = -1.5$, $a_6 = -4$, $a_7 = -4.9$, $a_8 = 2.5$ and $a_9 = 0$. a_6 and a_9 have quite a counteracting effect on the attractor and produces nearly opposite bifurcation traces in their respective domains. With the other parameters defaulted, $-6 < a_6 \leq 0$ and $0 \leq a_9 < 8$ suffice for chaos. Using the above specified default values for each a_k, a variable-step size with a maximum step of 10^{-4}, a relative tolerance of 10^{-9} and an initial condition $\boldsymbol{x}(0) = (1, 3, 8)$, a unique solution of the system by the Runge-Kutta fifth-order method and fourth-order error estimates [46], is plotted in Fig. 1 The stated solution algorithm can be achieved by the *MathWorks ode45* function. Starting from the initial condition, it can be seen that the trajectory enters into some confined region of phase space and remains there as the system is unperturbed. On the *bottom-right* of the same figure, sensitivity to two slightly different initial points (1, 3, 8) and (1, 3, 8.001), can be readily observed.

III. EQUILIBRIUM POINTS ANALYSIS

An equilibrium point $\boldsymbol{E}_p \in \mathbb{R}^3$, of system (1) is a point in phase space where $\dot{\boldsymbol{x}} = 0$. To find such a point, we solve

$$\begin{aligned} a_1x_1 + a_2x_1x_3 + a_3x_2x_3 &= 0 \\ a_4x_2 + a_5x_1x_3 + a_6 &= 0 \\ a_7x_3 + a_8x_1^2x_2 + a_9 &= 0. \end{aligned} \tag{2}$$

By symbolic solution method, it can be seen that Eq. (2) has seven points for which $\dot{\boldsymbol{x}} = 0$. Using the system parameters as stated in Section II, these points are computed to be:

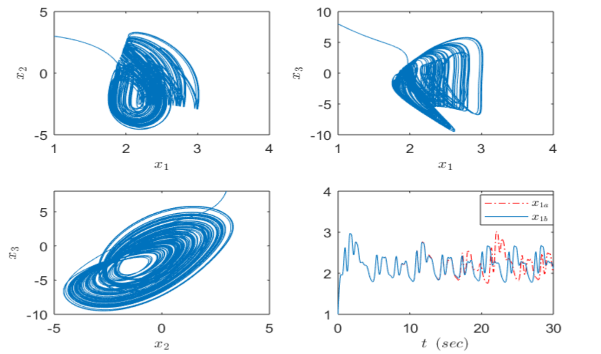

FIGURE 1. Phase portraits of system (1) projected on the $x_1 - x_2$ plane (*top left*), on the $x_1 - x_3$ plane (*top right*) and on the $x_2 - x_3$ plane (*bottom left*); initial condition was $x(0) = (1, 3, 8)$. On the *bottom right* are x_1 chaotic time series with initial conditions $x_a(0) = (1, 3, 8)$ and $x_b(0) = (1, 3, 8.001)$.

$$\begin{aligned} \boldsymbol{E}_1 &= (1.9828, -1.9360, -3.8835), \\ \boldsymbol{E}_2 &= (0.6297, 1.0785, 0.2182), \\ \boldsymbol{E}_3 &= (-3.3874, 0.1189, 0.6960), \\ \boldsymbol{E}_4 &= (-2.1769, 0.3391, 0.8199), \\ \boldsymbol{E}_5 &= (0.0000, 1.0256, 0.0000), \\ \boldsymbol{E}_6 &= (-b_1 - jc_1, b_2 + jc_2, -b_3 - jc_3), \\ \boldsymbol{E}_7 &= (-b_1 + jc_1, b_2 - jc_2, -b_3 + jc_3), \end{aligned} \tag{3}$$

where $b_1 = 0.5241$, $c_1 = 1.5955$, $b_2 = 0.7126$, $c_2 = 1.5818$, $b_3 = 2.1753$, $c_3 = 1.2247$, $j = \sqrt{-1}$. It can be noted that the system has five *real* equilibrium points and two *complex equilibrium points*.

In order to ascertain the stability property in the neighborhood of a *real* equilibrium point, we use the first Lyapunov's method, obtaining the system's Jacobian given by

$$J(\boldsymbol{x}) = \begin{pmatrix} a_1 + a_2\,x_3 & a_3\,x_3 & a_2\,x_1 + a_3\,x_2 \\ a_5\,x_3 & a_4 & a_5\,x_1 \\ 2\,a_8\,x_1\,x_2 & a_8\,x_1^2 & a_7 \end{pmatrix}. \tag{4}$$

Let $\lambda_p := \{\lambda_{i,p} | i = 1, 2, 3, p = 1, .., 5, \lambda_{i,p} \in \mathbb{C}\}$ be a set of eigenvalues at the equilibrium point $\boldsymbol{E}_p$. Also, given that I is a 3×3 identity matrix, the following is true:

$$det\Big(I\lambda_p - J(\boldsymbol{E}_p)\Big) = 0. \tag{5}$$

Eq. (5) is known as the characteristic equation. For each $\boldsymbol{E}_p$, Table 1 gives the elements of corresponding λ_p. It can be seen that each set $Re(\lambda_p)$, has at least an element in both the right-half and the left-half planes. Hence, the *real* equilibrium points are *saddle points*.

The stability transition near $\boldsymbol{E}_4$ for $-6 \leq a_6 \leq 1$ is shown in Fig. 2. The marker "*Ref*" is for extrapolation and comparison of $Re(\lambda_4)$ with results in Table 1. It can be seen that $\boldsymbol{E}_4$ is largely unstable in the domain of interest. Other equilibrium points have similar behaviors in the domain.

TABLE 1. Eigenvalues corresponding to each E_p.

E_p	$\lambda_{1,p}$	$\lambda_{2,p}$	$\lambda_{3,p}$
E_1	-3.56	$0.94 + j4.44$	$0.94 - j4.44$
E_2	-4.99	0.15	3.77
E_3	12.41	-0.04	-13.35
E_4	7.14	0.06	-8.19
E_5	-0.1	3.9	-4.9

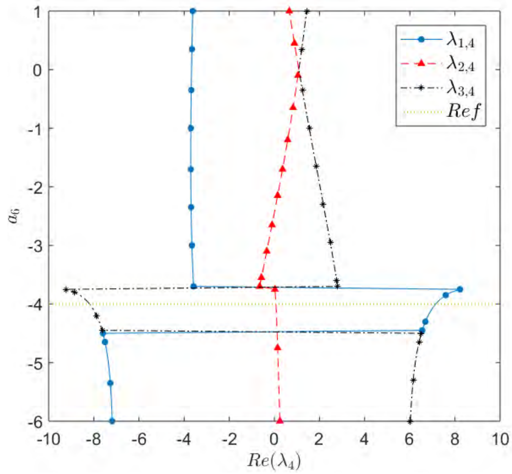

FIGURE 2. The stability behavior of E_4 as a_6 is varied in a domain of interest. It shows that E_4 remains unstable in the parameter domain.

IV. BASIN OF ATTRACTION

A basin of attraction is a set of points from any of which the system's trajectory starts, it ultimately enters a confined region of phase space. The set of points in this confined region is called the attractor [47], [48]. The system's dynamics remains in the attractor provided the system is unperturbed.

The basin of attraction of the present system is computed based on a root-finding algorithm, viz. the multidimensional *Newton-Raphson's method* [49] which can be expressed as:

$$x_{n+1} = x_n - J(x_n)^{-1} f(x_n), \quad (6)$$

where $n = 0, 1, .., N_{iter}$, N_{iter} is the number of iterations, $f(x_n) = \dot{x}_n$, other terms are as previously defined. Fig. 3 is an excerpt of the attraction basin along the $x_1 - x_2$ plane with

$$x_3(0) = \left\{ -6 + \frac{12}{49}(n-1) \mid n = 1, 2, .., 50 \right\}, \quad (7)$$

which is an *arithmetic sequence*. The cardinalities of the sets $x_1(0)$ and $x_2(0)$ are each 150. Therefore, $150^2 \times 50 = 1125000$ confined points are used in succession as initial seed or x_0. A point is designated by a cyan dot if it finds a root within an error of 10^{-12} otherwise it is designated by a black dot. The black patches are regions of phase space from which the system's trajectory could become unstable or at the peripheries, have a prolonged transient before identifying the attractor. The cyan color is the system's attraction basin.

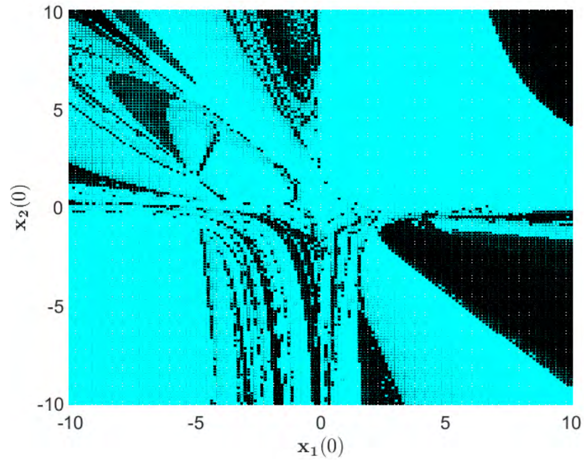

FIGURE 3. The basin of attraction on the $x_1 - x_2$ plane. (For the reference made to color, a web version or a color print is recommended).

V. ATTRACTOR TYPE

The attractor of a chaotic system can be *self-excited* or *hidden* [50], [51]. An attractor is self-excited if when a trajectory approaches a small neighborhood of an equilibrium, it processes a transient before it ultimately reaches the attractor. On the other hand, an attractor is hidden if its basin of attraction does not contain neighborhoods of any unstable equilibrium points [52], [53]. A stable equilibrium point of a chaotic system is not responsible for exciting the system's attractor, hence such an attractor is said to be *hidden*. Also, should a chaotic system have only *complex* equilibrium points, the associated attractor is *hidden* since the basin of attraction cannot contain a neighborhood of such points.

The system has two *complex* equilibrium points (E_6 and E_7), which may not contribute to the attractor's energy since they are *unphysical*. It also has five unstable *real* equilibrium points (namely E_1,.., E_5) which contribute to self-excitation of the attractor. Therefore, a trajectory in a small neighborhood of E_5 for example, processes a transient before identifying the attractor (see Fig. 4). Hence, the attractor is self-excited.

VI. BIFURCATION AND MAXIMAL LYAPUNOV EXPONENTS

Investigating bifurcation in a dynamical system can reveal a point where a qualitative change occurs in the system's behaviors. For instance, it can indicate a point where the system's solution transitions from a certain degree of periodicity to another. Also, the Lyapunov exponent presents an important characterization of a dynamical system. It reveals the average rate of separation of nearby orbits in phase space with a positive exponent indicating divergence of nearby orbits and a negative exponent indicating convergence of initially separated orbits. A chaotic system necessarily has a positive Lyapunov exponent. This is the principle behind the *sensitive dependence on initial conditions* of the chaotic dynamics.

The bifurcation and the maximal Lyapunov exponents were computed for a_6 varying from -10.0 to 2.0 and other

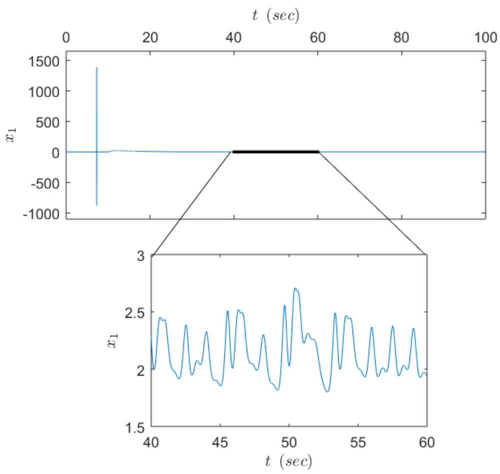

FIGURE 4. x_1 **time series with initial condition in a small neighborhood of** E_5**, precisely** $x(0) = E_5 + (0, 0, 0.001)$**. The trajectory processes a prolonged transient before identifying the attractor.**

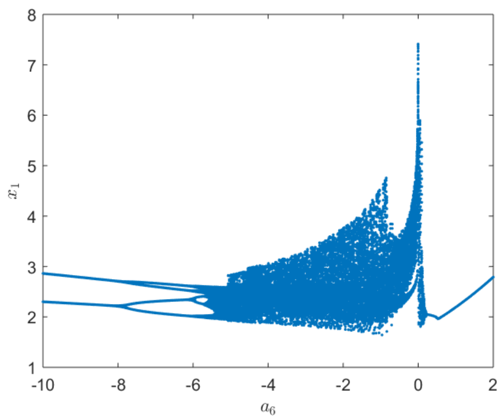

FIGURE 5. **Bifurcation in the system's dynamics with respect to varying** a_6 **parameter while other parameters remained as earlier defined.**

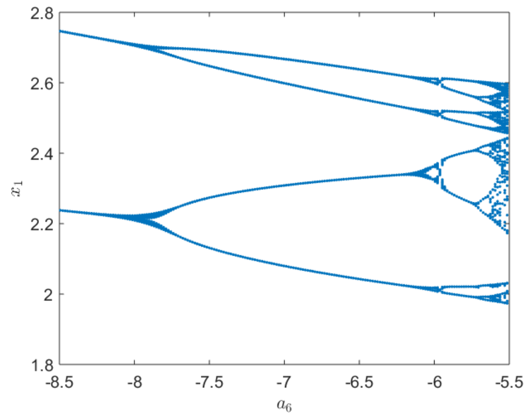

FIGURE 6. **A close-in view of Fig. 5.**

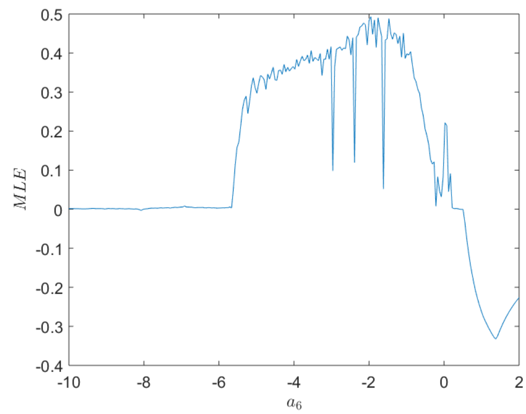

FIGURE 7. **The maximal Lyapunov exponents with respect to varying** a_6 **parameter.**

parameters as earlier stated. An initial condition on the attractor, precisely $\boldsymbol{x}(0) = (2.6440, 1.2352, 4.8727)$ was used in the computations in order to eliminate transients. From the left, chaotic dynamics starts by period-doubling bifurcation (Fig. 5). Fixing a_6, at -4 for example, and varying a_9 from -2 to 10 produces a similar and nearly opposite bifurcation trace with a slightly wider domain for chaos. Fig. 5 indicates a domain for possible chaotic event. Fig. 6 is a close-in view of the previous showing more clearly the initiation of chaos around $a_6 = -5.5$. Fig. 7 shows transition of the maximal Lyapunov exponents at every tiny step on a_6. A good agreement can be seen between Figs. 5 and 7. Extrapolating to the horizontal axis, it can be seen that for chaos $-6 < a_6 \leq 0$.

VII. LYAPUNOV SPECTRUM, DIMENSION, AND SYMMETRY

With $a_6 = -2$ since it is about a region of more intense chaos (see Fig. 7) and other parameters as previously stated, the Lyapunov spectrum of system (1) comprises $L_1 = 0.459$, $L_2 = -0.000$ and $L_3 = -1.782$ (see Fig. 8). These values can be calculated with the trajectory starting at $\boldsymbol{x}(0) = (2.6440, 1.2352, 4.8727)$ which lies on the attractor and performing 10^6 iterations. Convergence of elements of the spectrum is not dependent on initial conditions provided the initial conditions are in the attraction basin. Since $L_1 > 0$, the system can exhibit chaos. The Lyapunov dimension is given by $2 + (\frac{0.459}{1.782}) = 2.257$, which is fractional and the sum of elements in the Lyapunov spectrum is negative, that is, $\sum_{j=1}^{3} L_j = -1.323 < 0$. These imply that the system has a strange chaotic attractor that is dissipative. More precisely, the system decreases a volume in phase space by a factor of $\exp(-1.323) \approx 0.266$ per unit of time.

Furthermore, the system is not invariant with respect to rotation about any axes or with respect to reflection about any planes. However, the resultant system after such a transformation is equivalent to the original system. Moreover, provided the initial condition of the transformed system is correctly chosen, its solution only differs to the original system in accordance to the applied transformation.

VIII. REALIZATION AND PCB IMPLEMENTATION

In this section, the physical realization of the new chaotic system is presented to show its applicability. First, due to the limitations of electronic components, system (1) must be scaled. This can be achieved by the following

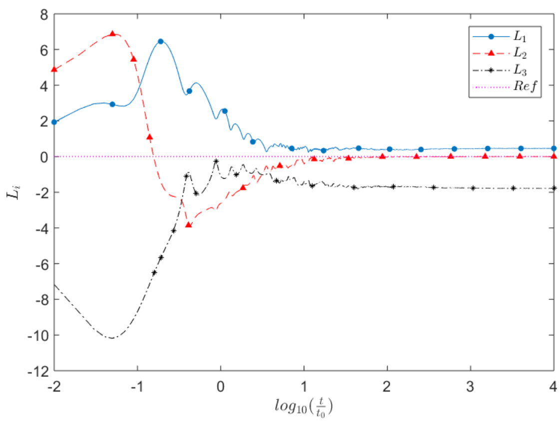

FIGURE 8. Spectrum of the Lyapunov exponents.

transformation:

$$w_i = \frac{1}{s_i}x_i, \quad (i = 1, 2, 3) \tag{8}$$

where each s_i is a positive real constant. By substituting (8) into (1) and considering that $a_9 = 0$, the following is obtained:

$$\begin{aligned}
\dot{w}_1 &= a_1 w_1 + s_3 a_2 w_1 w_3 + \frac{s_2 s_3}{s_1} a_3 w_2 w_3 \\
\dot{w}_2 &= a_4 w_2 + \frac{s_1 s_3}{s_2} a_5 w_1 w_3 + \frac{1}{s_2} a_6 \\
\dot{w}_3 &= a_7 w_3 + \frac{s_1^2 s_2}{s_3} a_8 w_1^2 w_2.
\end{aligned} \tag{9}$$

A possible realization of system (9) using operational amplifiers and analog multipliers is presented in Fig. 9. By applying Kirchhoff's laws to the circuit (Fig. 9), we get

$$\begin{aligned}
\frac{dv_1}{dt} &= -\frac{1}{R_1 C_1} v_1 + \frac{1}{10 R_2 C_1 V} v_1 v_3 + \frac{1}{10 R_3 C_1 V} v_2 v_3 \\
\frac{dv_2}{dt} &= \frac{1}{R_4 C_2}\frac{R_{10}}{R_9} v_2 - \frac{1}{10 R_5 C_2 V} v_1 v_3 - \frac{1}{R_6 C_2} V_{cc} \\
\frac{dv_3}{dt} &= -\frac{1}{R_7 C_3} v_3 + \frac{1}{100 R_8 C_3 V^2} v_1^2 v_2,
\end{aligned} \tag{10}$$

where v_1, v_2, and v_3 are the output voltages of the operational amplifiers $J1A$, $J1C$ and $J1D$, respectively, and V denotes volts. In order to properly visualize the phase portraits on the oscilloscope, it is convenient to increase the frequency of oscillation of the system by a factor of κ without modifying its amplitude. This implies a scaling of time. Let us consider that this scaling has already been accomplished in Eq. (10). If $C = C_1 = C_2 = C_3$, then an algebraic manipulation can be done to rearrange Eq. (10) as follows.

$$\begin{aligned}
\frac{dv_1}{dt} &= \frac{1}{RC}\left[-\frac{R}{R_1} v_1 + \frac{R}{10 R_2 V} v_1 v_3 + \frac{R}{10 R_3 V} v_2 v_3 \right] \\
\frac{dv_2}{dt} &= \frac{1}{RC}\left[\frac{R}{R_4}\frac{R_{10}}{R_9} v_2 - \frac{R}{10 R_5 V} v_1 v_3 - \frac{R}{R_6} V_{cc} \right] \\
\frac{dv_3}{dt} &= \frac{1}{RC}\left[-\frac{R}{R_7} v_3 + \frac{R}{100 R_8 V^2} v_1^2 v_2 \right],
\end{aligned} \tag{11}$$

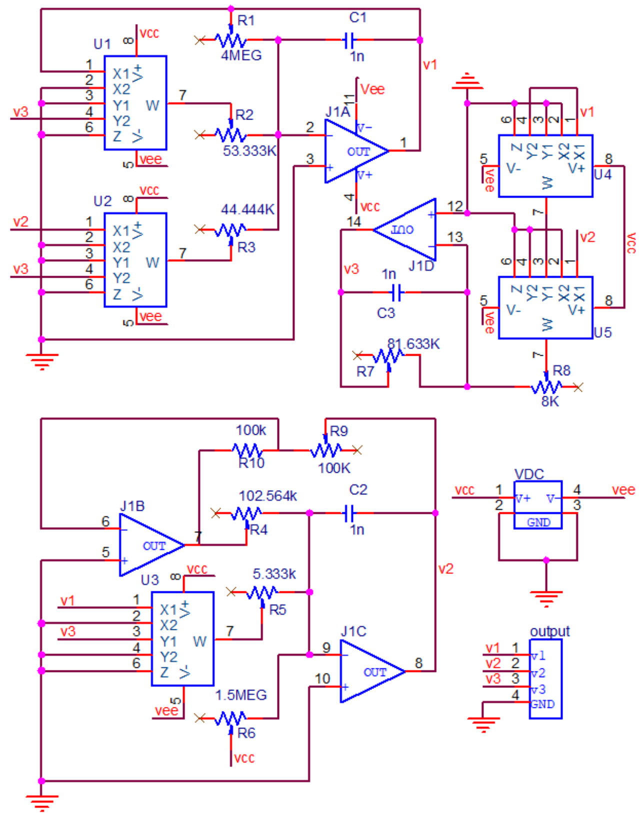

FIGURE 9. Circuit schematic of system (10).

where R is a value of a resistor to be determined. It can be established that

$$\kappa = \frac{1}{RC}. \tag{12}$$

Besides, the rescaling of time can be defined by means of the following relationship:

$$\tau = \kappa t = \frac{t}{RC}. \tag{13}$$

Finally, by substituting (13) into (11), the following dimensionless system can be obtained.

$$\begin{aligned}
\dot{W}_1 &= -\frac{R}{R_1} W_1 + \frac{R}{10 R_2} W_1 W_3 + \frac{R}{10 R_3} W_2 W_3 \\
\dot{W}_2 &= \frac{R}{R_4}\frac{R_{10}}{R_9} W_2 - \frac{R}{10 R_5} W_1 W_3 - \frac{R}{R_6}\frac{V_{cc}}{V} \\
\dot{W}_3 &= -\frac{R}{R_7} W_3 + \frac{R}{100 R_8} W_1^2 W_2,
\end{aligned} \tag{14}$$

where W_1, W_2 and W_3 correspond to the voltage signals v_1, v_2 and v_3, respectively. Let us consider that the frequency of oscillation of the chaotic system must be increased by a factor of $\kappa = 2500$. If we choose $C = 1nF$, then according to Eq. (12), $R = 400k\Omega$. It should be noted that for a higher frequency, a larger value of κ (or capacitors of smaller capacitances) can be used. However, κ may not be increased indefinitely due to device limitations. Besides, for "too" high frequencies, parasitic capacitance effect may set

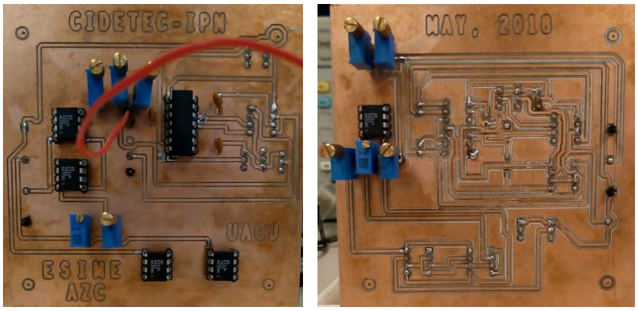

FIGURE 10. Hardware realization of the system. *Left:* top layer, *right:* bottom layer.

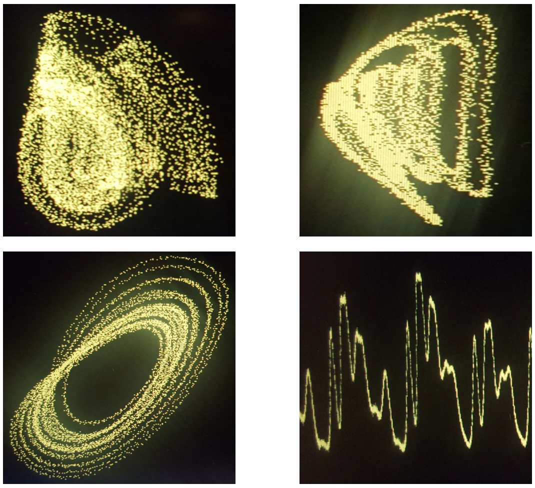

FIGURE 11. Circuit responses: $v_1 - v_2$ portrait corresponding to $x_1 - x_2$ portrait *(top-left)*, $v_1 - v_3$ portrait corresponding to $x_1 - x_3$ portrait *(top-right)*, $v_2 - v_3$ portrait corresponding to $x_2 - x_3$ portrait *(bottom-left)* and v_1 corresponding to the x_1 time-series *(bottom-right)*.

in. Also, let us consider that $s_1 = s_2 = 1$ and $s_3 = 5$. By taking the parametric values of system (1) as in Section II, if the corresponding coefficients of Eqs. (11) and (14) are compared, the following values of resistances can be gotten: $R_1 = 4M\Omega$, $R_2 = 53.333k\Omega$, $R_3 = 44.444k\Omega$, $R_4 = 102.564k\Omega$, $R_5 = 5.333k\Omega$, $R_6 = 1.5M\Omega$, $R_7 = 81.633k\Omega$, $R_8 = 8k\Omega$, $R_9 = R_{10} = 100k\Omega$. With these values and with the initial condition $v_1(0) = 1$, $v_2(0) = 3$, $v(0) = 8/5$, the circuit (Fig. 9) is simulated by *PSpice* and the phase planes are in good agreement with Fig. 1.

Implementation of the circuit (Fig. 9) was done on a printed circuit board (PCB), which is displayed in Fig. 10. *OrCAD-Capture* was used for schematic layout and *Netlist* generation and then *Allegro PCB Designer* was used to lay out the footprints. Finally, a table-top CNC[1] machine was used for drilling and engraving a copper board to produce the PCB.

Some responses from the system's hardware are shown in Fig. 11. It can be seen that the hardware circuit responses agree with the numerical Runge-Kutta solution of Fig. 1.

[1]Computer Numerical Control

IX. WELCH SPECTRAL ANALYSIS OF THE EXPERIMENTAL DATA

The Welch method offers quite a reduced variance of the power spectral density (PSD) estimate. Hence, it is an estimator of choice over a number of others. It entails averaging of windowed periodograms derived from successive overlapping segments which are actually sequential subsamples of the data sequence of interest. The Welch's PSD estimate [55] for K segments, each of length M is given by

$$P_{WE}(\nu) = \frac{1}{K}\sum_{k=1}^{K}\sum_{m=1}^{M}\frac{1}{w(m)^2}|Y_k(\nu)|^2, \tag{15}$$

where $w(m)$ is the window function, ν is frequency in Hz and $Y_k(\nu)$ is a windowed discrete Fourier transform of the subsample y_k. It can be expressed as

$$Y_k(\nu) = \sum_{m} y_k(m)w(m)\exp(-j2\pi\nu m). \tag{16}$$

The collected experimental data has a record length of $N = 2500$ samples and a sample interval in *seconds* of $T = 2 \times 10^{-5}$. Hence, the data is sampled at 2500 samples per $NT = 0.05$ *seconds*. That is, the sampling frequency is $50kHz$. Therefore, *time* can be expressed according to the following recurrence relation:

$$t_n = t_0 + nT, \quad n = 0, 1, .., N-1, \tag{17}$$

with $t_0 = T$. Based on this, the experimental data can be represented as a sequence $y(t_n)$. This sequence is partitioned into K overlapping segments with the maximum length of a segment being M samples. The segments are used as inputs to the Welch's algorithm presented earlier in this section.

A chaotic signal should have no *periodicities*. Instead, it should have a broad continuous spectrum. Hence, we analyze the experimental data using Welch spectral estimator in order to verify its aperiodicity. First, let us recall that the spectral density estimate of a noise-like signal bearing some well-defined periodic signals looks like Fig. 12. The frequency components are distinct and have steady intensity with time. But for a chaotic signal, a distinct component is not observed in the frequency domain. Due to this property, a chaotic signal can be used as information shield in a communication application. In estimating the PSD of the experimental data, we choose a window with a side lobe attenuation parameter small enough to not mask any possible low amplitude periodicities and with size, large enough to give good frequency resolution. Hence, we choose a Kaiser window of length $M = 500$ and side lobe attenuation less than $21dB$, and $K = 5$ segments. Each segment has the second half of its samples (i.e. 50 percent of M) overlapping with the next segment. With $y(t_n) = v_2$, that is, an experimental time series, Fig. 13 shows a PSD estimate and a spectrogram made using the above settings. No frequency peaks can be seen in the PSD plot nor a steady intensity in the spectrogram. The side lobes are clearly not masking any possible periodicities. Hence, the experimental data are intrinsically aperiodic.

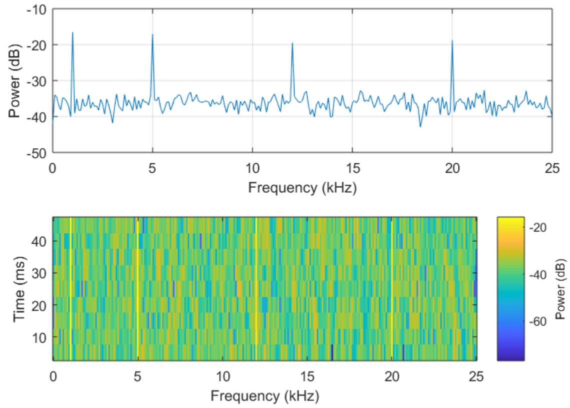

FIGURE 12. Welch PSD estimate (*top*) and a spectrogram of a four-tone multiply periodic signal in a noise-like signal.

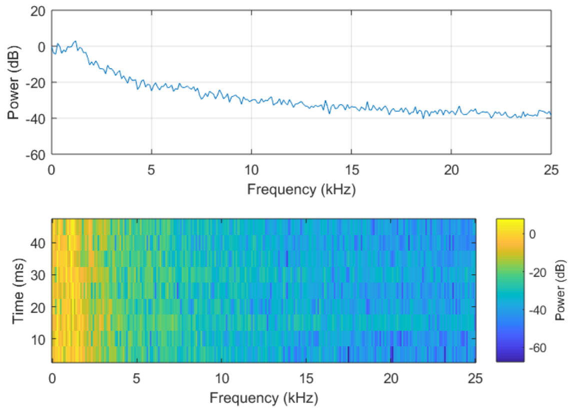

FIGURE 13. Welch PSD estimate (*top*) and a spectrogram both having a kaiser window of length 500 and side lobe attenuation less 21 *dB*.

X. CORRELATION DIMENSION FROM EXPERIMENTAL DATA

Having deduced in the previous section that the experimental data is aperiodic, we now must ensure that it is of deterministic chaos. Therefore, we analyze the data as follows.

Let us suppose that an attractor $\mathcal{A}$ is covered by reasonably small hyperspheres of radii $r = \{r_i | i = 1, 2 \ldots\}$. If the number of data points N, on the attractor is large, then for every pair of points $\boldsymbol{X}_j \in \mathcal{A} \subset \mathbb{R}^n$ ($j = 1, 2, .., N$ and n is the dimension of phase space), with a metric less than an r_i is a measure

$$C(r_i, N) = \lim_{N\to\infty} \frac{1}{N^2} \sum_{j=1}^{N-1} \sum_{k=j+1}^{N} H(r_i - ||\boldsymbol{X}_j - \boldsymbol{X}_k||), \quad (18)$$

which is called the correlation sum, H is the *Heaviside step function*. For some small r and large N, it has been shown that [56]:

$$C(r, N) \propto r^{D_2}, \quad (19)$$

where

$$D_2 := \lim_{r\to 0} \lim_{N\to\infty} \frac{\partial \ln C(r, N)}{\partial \ln r} \quad (20)$$

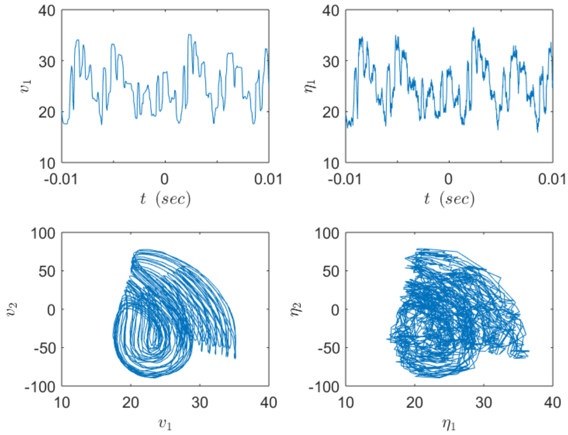

FIGURE 14. *Left:* time series and $v_1 - v_2$ phase portrait from experimental data. *Right:* corresponding plots with 3 *dB* noise.

is a measure of strangeness called the correlation dimension. Unfortunately, for relatively short data extract from say an experiment and for small length scales, the correlation sum presents a couple of challenges. Notably, the issue of temporal correlation of pairs entering the sums. If it exists, spurious effects in the correlation integral is present, which consequently undermines the integrity of the correlation dimension. To ameliorate the effect of correlated pairs, *J. Theiler* suggested discarding pairs of points whose temporal distances are less than a certain constant w, often called the *Theiler window*. With this consideration, the inner sums in Eq. (18) will be modified such that $|j - k| > w$. A space-time separation plot can help in the estimation of w. Next, we have to estimate a minimal embedding space $D_E \in \mathbf{Z}^+$ which can faithfully represent our data. Although the numerical time-series by the method of *false nearest neighbors* [57], indicates a $D_E = 3$ as minimally sufficient, the experimental time-series does not give a clear indication. Besides, we note that an attempt at reconstructing the physical phase space using the experimental data v_1, v_2 and v_3 in succession gives the estimated embeddings 4, 3 and 3, respectively. If we decide that $D_E = 3$ is a faithful embedding, embedology permits us to choose higher embedding spaces. And D_2 is expected to not significantly keep increasing with increasing D_E.

By the above understanding, the experimental data was collected for analysis. Fortunately, we do not have to use the reconstructed phase space since a vector of states are simultaneously available to us. In Fig. 14 (*left*) are plots from the experimental data. For the sake of comparison, on the *right* of same figure are the corresponding experimental signals plus 3 *dB* noise. Where η_1 and η_2 in the figure are noise corrupted data derived from v_1 and v_2, respectively. Using the noise-corrupted data as input to the *TISEAN* d_2 *binary* [58] and after smoothening the output, Fig. 15 shows a lack of correlation for different embedding spaces. D_2^* in this case is invalid. For the case with minimal noise, the multivariate experimental data was input to the d_2 binary with a time lag $\tau = 3$, and a Theiler window, $w = 125$, i.e. 5% of the sample

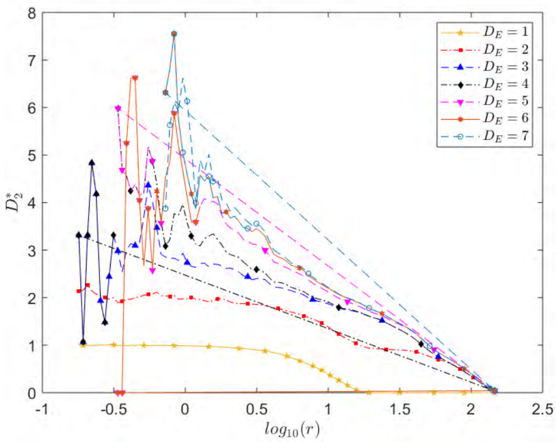

FIGURE 15. D_2^* **versus** ***log*****(*****r*****) depicting a lack of correlation in the 3*****dB*** **noise-corrupted experimental data. Theiler window,** $w = 125$ **and a time lag,** $\tau = 3$**.**

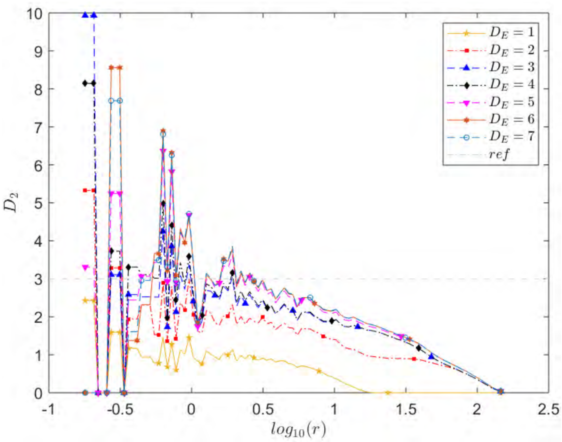

FIGURE 16. D_2 **versus** ***log*****(*****r*****) depicting existence of correlation in the experimental data. Theiler window,** $w = 125$ **and a time lag,** $\tau = 3$**.**

length. As can be seen in Fig. 16, a clear correlation exists for $0 \leq log_{10}(r) < 2.5$ and for $D_E = 3, .., 7$. Also, the *loglog* plots of the correlation sums versus the corresponding radii indicate power law behaviors (see Fig. 17). Following the *"ref"* line in Fig. 16, it can be seen that $D_2 < 3$. In particular $D_2 = 2.092$ as can be estimated by the least squares method (see Fig. 18). Being less than $n = 3$, the observed behavior in the experimental data is of deterministic chaos [59].

XI. INFORMATION MASKING BY THE CHAOTIC SIGNAL

Due to their sensitive dependence on initial conditions, chaotic systems' signals are information shield of innately high security integrity. The present system has yet another innate quality which makes its secure communication application simple. It has a property known as *self-synchronization*. Let us take Eq. (10) to be a *master* system. In theory, the v_1 and the v_2 signals should synchronize respectively subsystems (u_2, u_3) and (u_1, u_3) of corresponding *slave* systems since they both have negative sub-Lyapunov exponents [60]. In particular, the sub-Lyapunov exponents are $(-0.225659, -0.777087)$ and $(-0.269054, -4.952959)$,

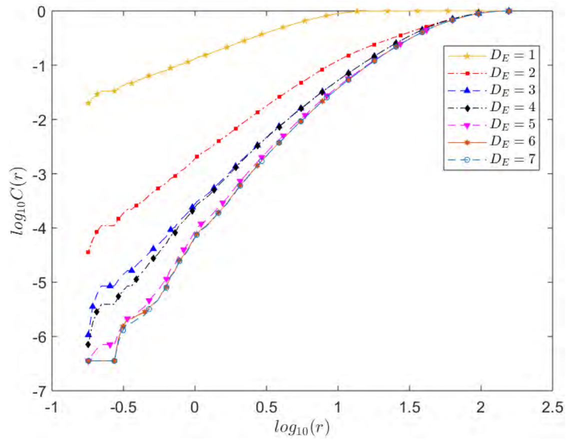

FIGURE 17. **The** ***loglog*** **plots of correlation sums versus corresponding radii.**

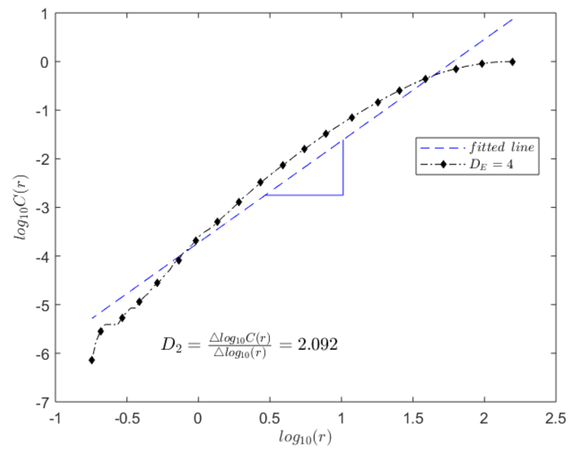

FIGURE 18. **Least squares fitting for estimating slope of the curve.**

respectively. Synchronization is aimed at making the *slave* system's trajectory to follow the *master's* as time approaches infinity for arbitrary initial conditions. Let us consider the *slave* subsystem

$$\dot{u}_2 = \frac{u_2}{R_{11}C_4}\frac{R_{17}}{R_{16}} - \frac{v_1 u_3}{10R_{12}C_4 V} - \frac{1}{R_{13}C_4}V_{cc}$$
$$\dot{u}_3 = -\frac{u_3}{R_{14}C_5} + \frac{v_1^2 u_2}{100R_{15}C_5 V^2}, \quad (21)$$

where parameters such as resistances and capacitances are assumed equal to corresponding *master* system parameters. But initial charges on corresponding capacitors are in general unequal and may also be unknown. Since the system is chaotic, the signals of the *master* and the *slave* systems should become increasingly uncorrelated. However, this will not happen because the *master* signal v_1, which has self-synchronizing capability, is coupled to the *slave* system (see Fig. 19). Thus, the *slave* system's trajectory follows the *master's* after a short period of time (see Fig. 20).

With synchronization of the *master-slave* configuration achieved, information masking by a *master* chaotic signal and the subsequent recovery at the *slave system* becomes

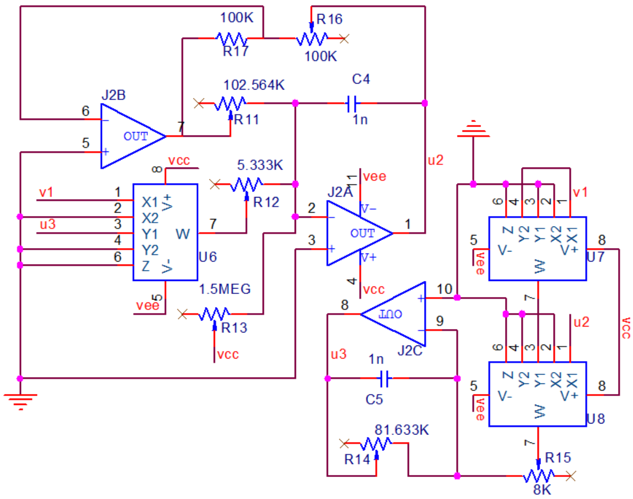

FIGURE 19. The slave system coupled to the master system via the v_1 signal.

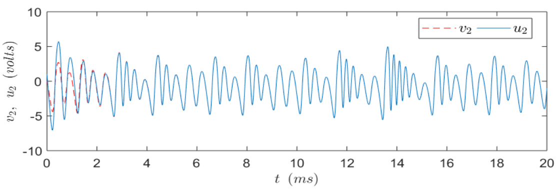

FIGURE 20. Slave system signal u_2 synchronizes to the master signal v_2.

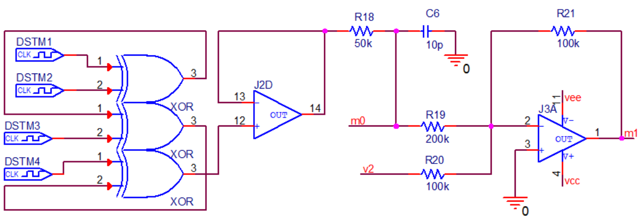

FIGURE 21. Modulation of the information signal m_0 onto the *master* v_2 chaotic signal.

possible [54]. For example, let us assume an information source provided by the array of digital stimuli $DSTM1, .., DSTM4$ (see Fig. 21 and Table 2) which are *XORed* to give a nontrivial square wave m_0 which can represent a bit of information. For privacy of m_0 as it is been transmitted, it can be masked by a chaotic signal. Fig. 21 shows modulation of m_0 onto the v_2 chaotic signal. The unit gain element $J2D$, in the figure serves as a buffer to the information source which changes between a '*high*' and a '*low*' states. Eq. (22) is the mathematical expression for the information modulation.

$$m_1 = -\frac{m_0}{2} - v_2. \qquad (22)$$

The result m_1 (Fig. 22) can be transmitted by any standard means to the *slave* system. By virtue of the established synchronization, the *slave* system signal u_2 has the necessary *chaotic code* to recover the masked information. Eq. (23) is the algebraic expression for the information demodulation

TABLE 2. Properties and values (in millisecond) of the various digital stimuli.

	Off-time	On-time	Time delay, t_d
DSTM1	4.0	3.0	5.0
DSTM2	5.0	0.5	5.0
DSTM3	4.0	1.0	5.0
DSTM4	3.5	1.0	5.0

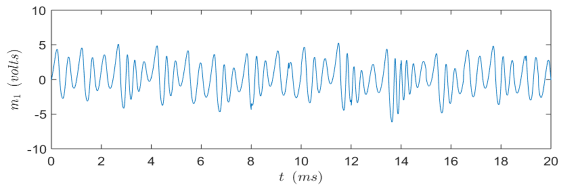

FIGURE 22. The transmitted signal bearing the information signal.

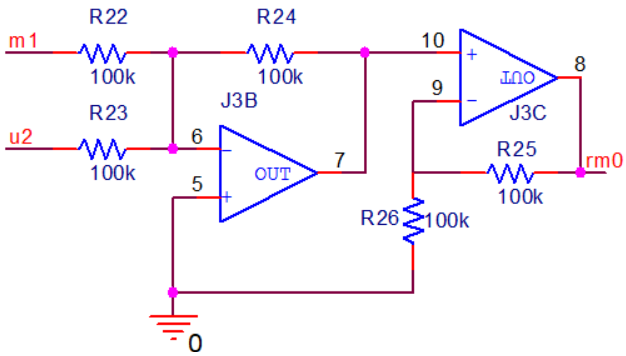

FIGURE 23. Demodulation of the signal shielded in m_1.

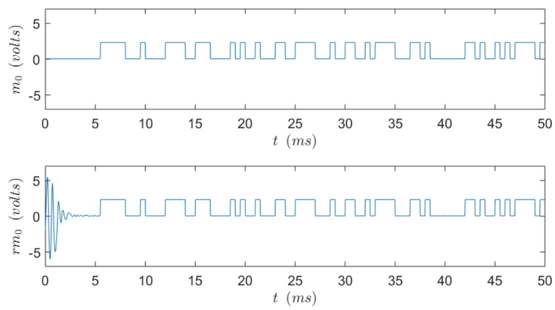

FIGURE 24. rm_0 synchronizes to the original information signal m_0 in less than 5 *millisecond*.

(see Fig. 23).

$$rm_0 = -2m_1 - 2u_2. \qquad (23)$$

In order to not lose a relevant part of the information before synchronization is achieved, the *delay time* t_d of the message source can be extended appropriately. Presently, we have used $t_d = 5.0$ *millisecond*. As can be seen in Fig. 24, the *slave* system recovers the *original* signal m_0 with an error $rm_0 - m_0$. In general, time evolution of the error is given by

$$\lim_{t\to\infty} rm_0 - m_0 = 0. \qquad (24)$$

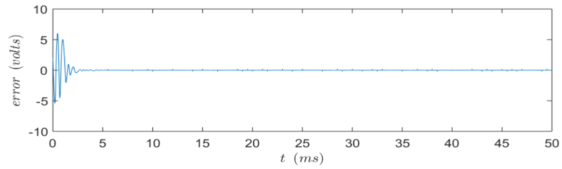

FIGURE 25. The information recovery error.

It can be seen in Fig. 25 that the information recovery error converges to zero in less than 5 *millisecond*. Thus, substantiating the effectiveness of the design.

XII. CONCLUSION

We have presented a new 3-dimensional autonomous nonlinear dynamical system. Simulation shows that the system has spatially bounded aperiodic orbits and exhibits sensitive dependence on initial conditions. Also, the system is dissipative and has a fractional Lyapunov dimension. Hence, the system possesses a chaotic strange attractor. Further, it is shown by means of PCB implementation that the system is viable for use in analog electronic application. In addition, the aperiodicity of the experimental data is confirmed by the Welch method. Moreover, experimental time series of the system is used to estimate a correlation dimension which turns out to be less than the system's degree of freedom thus confirming that the hardware system responses are of deterministic chaos. Finally an electronic circuit design of a secure communication application involving a *slave-master* configuration shows that a digital signal modulated by a *master* system signal can be recovered by the *slave* system within a period of 5 *milliscond*. Thus, confirming the effectiveness of the electronic realization. To obtain a greater flexibility, in a future work, this system will be implemented on FPGA as the basis of a secured software-defined radio.

ACKNOWLEDGMENT

The authors would like to thank Centro de Investigación en Ciencia y Tecnología Aplicada (CICTA) of Universidad Autónoma de Ciudad Juárez for the equipment and facilities. Likewise, they are grateful to the Instituto Politécnico Nacional, and CONACYT. In particular, we must recognize the managerial support provided by ESIME-Azc principal, Ing. José Armando Rodríguez Mena, toward the realization of this project. Likewise, thanks should be given to Dr. Gabriel Sepulveda Cervantes for allowing use of his laboratory's CNC machine and other resources, to Dr. Miguel Gabriel Villarreal Cervantes for making his laboratory's resources available during the development of this work, and to Mr. Martin Cordero for his technical support and discussions in the making of the PCB. They also thank Dr. Juan L. Mata-Machuca for assisting with a modern oscilloscope which allowed USB storage of experimental data. Finally, they recognize the time and efforts of the anonymous reviewers. They appreciate their invaluable comments which have improved the manuscript.

REFERENCES

[1] K. Aihara, "Chaos and its applications," *Procedia IUTAM*, vol. 5, pp. 199–203, Jan. 2012.

[2] H. Nomura, N. Wakami, and S. Kondo, "Non-linear technologies in a dishwasher," in *Proc. IEEE Int. Fuzzy Syst. Int Joint Conf., 4th IEEE Int. Conf. Fuzzy Syst., 2nd Int. Fuzzy Eng. Symp.*, vol. 5, Mar. 1995, pp. 57–58.

[3] H. R. Pourshaghaghi, B. Kia, W. Ditto, and M. R. Jahed-Motlagh, "Reconfigurable logic blocks based on a chaotic Chua circuit," *Chaos, Solitons, Fractals*, vol. 41, no. 1, pp. 233–244, 2009.

[4] T. Munakata, S. Sinha, and W. L. Ditto, "Chaos computing: Implementation of fundamental logical gates by chaotic elements," *IEEE Trans. Circuits Syst. I, Fundam. Theory Appl.*, vol. 49, no. 11, pp. 1629–1633, Nov. 2002.

[5] Y. Horio and K. Aihara, "Analog computation through high-dimensional physical chaotic neuro-dynamics," *Phys. D, Nonlinear Phenomena*, vol. 237, no. 9, pp. 1215–1225, 2008.

[6] Y. Horio, T. Ikeguchi, and K. Aihara, "A mixed analog/digital chaotic neuro-computer system for quadratic assignment problems," *Neural Netw.*, vol. 18, nos. 5–6, pp. 505–513, 2005.

[7] A. Akgul, I. Moroz, I. Pehlivan, and S. Vaidyanathan, "A new four-scroll chaotic attractor and its engineering applications," *Optik*, vol. 127, no. 13, pp. 5491–5499, 2016.

[8] M. A. Jafari *et al.*, "Chameleon: The most hidden chaotic flow," *Nonlinear Dyn.*, vol. 88, no. 3, pp. 2304–2317, 2017.

[9] X. Zang, S. Iqbal, Y. Zhu, X. Liu, and J. Zhao, "Applications of chaotic dynamics in robotics," *Int J. Adv. Robot. Syst.*, vol. 13, no. 2, p. 60, 2016.

[10] U. Nehmzow and K. Walker, "Quantitative description of robot–environment interaction using chaos theory," *Robot. Auton. Syst.*, vol. 53, nos. 3–4, pp. 177–193, 2005.

[11] Z. Merali. (Jan. 2010). Robotic roach creates order from chaos. Nature News. Accessed: Apr. 4, 2018. [Online]. Available: https://www.nature.com/news/2010/100117/full/news.2010.15.html

[12] L. M. Pecora and T. L. Carroll, "Synchronization of chaotic systems," *Chaos*, vol. 25, no. 9, p. 097611, 2015.

[13] S. Vaidyanathan *et al.*, "A new chaotic attractor with two quadratic nonlinearities, its synchronization and circuit implementation," *IOP Conf. Mater. Sci. Eng.*, vol. 332, no. 1, 2018, p. 012048.

[14] S. Vaidyanathan, "A new 3-D jerk chaotic system with two cubic nonlinearities and its adaptive backstepping control," *Arch Control Sci.*, vol. 27, no. 3, pp. 409–439, 2017.

[15] T. Wang, D. Wang, and K. Wu, "Chaotic adaptive synchronization control and application in chaotic secure communication for industrial Internet of Things," *IEEE Access*, vol. 6, pp. 8584–8590, 2018.

[16] Z. Zhao, F. Lv, J. Zhang, and Y. Du, "H_∞ synchronization for uncertain time-delay chaotic systems with one-sided Lipschitz nonlinearity," *IEEE Access*, vol. 6, pp. 19798–19806, 2018.

[17] Y. Wang, Y. Zhu, H. R. Karimi, and X. Li, "Sampled-data exponential synchronization of chaotic Lur'e systems," *IEEE Access*, vol. 5, pp. 17834–17840, 2017.

[18] G. Kaddoum, "Wireless chaos-based communication systems: A comprehensive survey," *IEEE Access*, vol. 4, pp. 2621–2648, May 2016.

[19] C. Bai, H. Ren, C. Grebogi, and M. S. Baptista, "Chaos-based underwater communication with arbitrary transducers and bandwidth," *Appl. Sci.*, vol. 8, no. 2, p. 162, 2018.

[20] J. Y. Duan and H. Yang, "Phase-orthogonality CDSK: A reliable and effective chaotic communication scheme," *IET Commun.*, vol. 12, no. 9, pp. 1116–1122, 2018.

[21] A. Argyris, E. Grivas, M. Hamacher, A. Bogris, and D. Syvridis, "Chaos-on-a-chip secures data transmission in optical fiber links," *Opt. Express*, vol. 18, no. 5, pp. 5188–5198, Feb. 2010.

[22] V. Annovazzi-Lodi, G. Aromataris, M. Benedetti, and S. Merlo, "Secure chaotic transmission on a free-space optics data link," *IEEE J. Quantum Electron.*, vol. 44, no. 11, pp. 1089–1095, Nov. 2008.

[23] S. Donati and C. R. Mirasso, "Introduction to the feature section on optical chaos and applications to cryptography," *IEEE J. Quantum Electron.*, vol. 38, no. 9, pp. 1138–1140, Sep. 2002.

[24] J. L. Mata-Machuca and R. Aguilar-López, "Adaptative synchronization in multi-output fractional-order complex dynamical networks and secure communications," *Eur. Phys. J.*, vol. 133, no. 1, p. 14, 2018.

[25] B. Gopalakrishnan and M. A. Bhagyaveni, "Anti-jamming communication for body area network using chaotic frequency hopping," *Healthcare Technol. Lett.*, vol. 4, no. 6, pp. 233–237, 2017.

[26] U. E. Kocamaz, S. Çiçek, and Y. Uyaroğlu, "Secure communication with chaos and electronic circuit design using passivity-based synchronization," *J. Circuit Syst. Comput.*, vol. 27, no. 4, pp. 1–20, 2018.
[27] D. Rickles, P. Hawe, and A. Shiell, "A simple guide to chaos and complexity," *J. Epidemiol Community Health*, vol. 61, no. 11, pp. 933–937, 2007.
[28] D. Bazeia, M. B. P. N. Pereira, A. V. Brito, B. F. De Oliveira, and J. G. G. S. Ramos, "A novel procedure for the identification of chaos in complex biological systems," *Sci. Rep.*, vol. 7, p. 44900, Mar. 2017.
[29] V. Basios and Y. Gunji, "Chaotic dynamics in biological information processing: Revisiting and revealing its logic (a mini-review)," *Opera Med. Physiol.*, vol. 3, nos. 1–13, 2017.
[30] I. R. Epstein and K. Showalter, "Nonlinear chemical dynamics: Oscillations, patterns, and chaos," *J. Phys. Chem*, vol. 100, no. 31, pp. 13132–13147, 1996.
[31] F. J. Muzzio and M. Liu, "Chemical reactions in chaotic flows," *Chem. Eng. J.*, vol. 64, no. 1, pp. 117–127, 1996.
[32] N. S. Postnikov, "Conditions for the existence of chaotic oscillations in nuclear reactors," *At. Energy*, vol. 88, no. 6, pp. 449–455, 2000.
[33] M. Faggini, "Chaotic time series analysis in economics: Balance and perspectives," *Chaos*, vol. 24, no. 4, p. 042101, 2014.
[34] S. R. Mann, "Chaos theory and strategic thought," *Parameters*, vol. 22, no. 3, p. 54, 1992.
[35] J. L. Mata-Machuca, R. Martínez-Guerra, and R. Aguilar-López, "Monitoring in a predator–prey systems via a class of high order observer design," *BioSystems*, vol. 100, no. 1, pp. 65–69, 2010.
[36] Z. Aram, S. Jafari, J. Ma, J. C. Sprott, S. Zendehrouh, and V. Pham, "Using chaotic artificial neural networks to model memory in the brain," *Commun. Nonlinear Sci. Numer Simul.*, vol. 44, pp. 449–459, Mar. 2017.
[37] J. J. Rubio, "Stable Kalman filter and neural network for the chaotic systems identification," *J. Franklin Inst*, vol. 354, no. 16, pp. 7444–7462, 2017.
[38] J. M. Cushing, S. M. Henson, R. A. Desharnais, B. Dennis, R. F. Costantino, and A. King, "A chaotic attractor in ecology: Theory and experimental data," *Chaos, Solitons Fractals*, vol. 12, no. 2, pp. 219–234, 2001.
[39] P. Gholamin and A. H. R. Sheikhani, "A new three-dimensional chaotic system: Dynamical properties and simulation," *Chin. J. Phys.*, vol. 55, no. 4, pp. 1300–1309, 2017.
[40] J. Lü, G. Chen, and D. Cheng, "A new chaotic system and beyond: The generalized Lorenz-like system," *Int. J. Bifucation Chaos*, vol. 14, no. 5, pp. 1507–1537, 2004.
[41] Lü, Jinhu and G. Chen, "A new chaotic attractor coined," *Int. J. Bifucation Chaos*, vol. 12, no. 3, pp. 659–661, 2002.
[42] P. Zhou and M. Ke, "A new 3D autonomous continuous system with two isolated chaotic attractors and its topological horseshoes," *Complex*, vol. 2017, Nov. 2017, Art. no. 4037682.
[43] J. Lü, G. Chen, and S. Zhang "Dynamical analysis of a new chaotic attractor," *Int. J. Bifucation Chaos*, vol. 12, no. 5, pp. 1001–1015, 2002.
[44] W. Liu and G. Chen, "A new chaotic system and its generation," *Int J. Bifurcation Chaos*, vol. 13, no. 1, pp. 261–267, 2003.
[45] J. C. Sprott, "Some simple chaotic flows," *Phys. Rev. E, Stat. Phys. Plasmas Fluids Relat. Interdiscip. Top.*, vol. 50, no. 2, p. R647, 1994.
[46] J. R. Dormand and P. J. Prince, "A family of embedded Runge-Kutta formulae," *J. Comput. Appl. Math.*, vol. 6, no. 1, pp. 19–26, 1980.
[47] S. H. Strogatz, "Strange attractors," in *Nonlinear Dynamics and Chaos: With Applications to Physics, Biology, Chemistry, and Engineering*, 1st ed. Cambridge, MA, USA: Perseus Books, 1994, ch. 12, sec. 12.1, pp. 429–430.
[48] K. T. Alligood, T. D. Sauer, and J. A. Yorke, "Chaotic attractors," in *Chaos: An Introduction to Dynamical Systems*, 1st ed. New York, NY, USA: Springer-Verlag, 1996, ch. 6, sec. 6.1, pp. 231–240.
[49] A. Ben-Israel, "A Newton-Raphson method for the solution of systems of equations," *J. Math. Anal. Appl.*, vol. 15, no. 2, pp. 243–252, 1966.
[50] J. C. Sprott, "Strange attractors with various equilibrium types," *Eur. Phys. J. Special Topics*, vol. 224, no. 8, pp. 1409–1419, 2015.
[51] D. Dudkowski, S. Jafari, T. Kapitaniak, N. V. Kuznetsov, G. A. Leonov, and A. Prasad, "Hidden attractors in dynamical systems," *Phys. Rep.*, vol. 637, pp. 1–50, Jun. 2016.
[52] A. Akgul and I. Pehlivan, "A new three-dimensional chaotic system without equilibrium points, its dynamical analyses and electronic circuit application," *Tech. Gazette*, vol. 23, no. 1, pp. 209–214, 2016.
[53] N. V. Kuznetsov and G. A. Leonov, "Hidden attractors in dynamical systems: Systems with no equilibria, multistability and coexisting attractors," *IFAC Proc. Volumes*, vol. 47, no. 3, pp. 5445–5454, 2014.
[54] J. P. Singh and B. K. Roy, "Hidden attractors in a new complex generalised Lorenz hyperchaotic system, its synchronisation using adaptive contraction theory, circuit validation and application," *Nonlinear Dyn.*, vol. 92, no. 2, pp. 373–394, 2018.
[55] E. C. Ifeachor and B. W. Jervis, "Modified periodogram methods," in *Digital Signal Processing: A Practical Approach*, 1st ed. Reading, MA, USA: Addison-Wesley, 1993, ch. 10, sec. 10.3.4, pp. 600–601.
[56] P. Grassberger and I. Procaccia, "Characterization of strange attractors," *Phys. Rev. Lett.*, vol. 50, no. 5, p. 346, 1983.
[57] M. B. Kennel, R. Brown, and H. D. I. Abarbanel, "Determining embedding dimension for phase-space reconstruction using a geometrical construction," *Phys. Rev. A, Gen. Phys.*, vol. 45, no. 6, pp. 3403–3411, Mar. 1992.
[58] R. Hegger, H. Kantz, and T. Schreiber, "Practical implementation of nonlinear time series methods: The TISEAN package," *Chaos, Interdiscipl. J. Nonlinear Sci.*, vol. 9, no. 2, pp. 413–435, 1999.
[59] P. Grassberger and I. Procaccia, "Measuring the strangeness of strange attractors," *Physica D, Nonlinear Phenomena*, vol. 9, nos. 1–2, pp. 189–208, 1983.
[60] L. M. Pecora and T. L. Carroll, "Synchronization in chaotic systems," *Phys. Rev. Lett.*, vol. 64, no. 8, pp. 821–824, 1990.
[61] X. Wang, V. Pham, S. Jafari, C. Volos, J. M. Munoz-Pacheco, and E. Tlelo-Cuautle, "A new chaotic system with stable equilibrium: From theoretical model to circuit implementation," *IEEE Access*, vol. 5, pp. 8851–8858, 2017.

CHRISTIAN NWACHIOMA received the bachelor's degree in physics from the Federal University of Technology, Owerri, Nigeria, in 2010, and the M.Sc. degree in physics from the COMSATS University Islamabad, Pakistan, in 2016. He is currently pursuing the Ph.D. degree in robotics and mechatronic system engineering with the Instituto Politécnico Nacional, Mexico. His current research interests include chaos theory and control and chaos-theory-related innovations in communication and robotics.

J. HUMBERTO PÉREZ-CRUZ was born in Mexico. He received the Diploma degree in electronic engineering from the Oaxaca Institute of Technology, Mexico, in 1999, the M.S. degree in electronics engineering from the Toluca Institute of Technology, Mexico, in 2004, and the Ph.D. degree in automatic control from CINVESTAV, in 2008. He is currently a full-time Professor with the Instituto Politécnico Nacional and a member of the National System of Researchers (SNI) Level I, National Council of Science and Technology (CONACYT). He has published 28 papers in international journals, two chapters of international books, and 14 papers in international conferences. His research interests include adaptive control, chaotic systems, artificial neural networks, system modeling and identification, and finance.

ABIMAEL JIMÉNEZ received the M.S. and Ph.D. degrees in electronics engineering from the National Institute of Astrophysics, Optics and Electronics, Puebla, Mexico, in 2002 and 2008, respectively, for his work on modeling and simulation of dynamic threshold MOSFET. From 2008 to 2009, he was a Professor with the University of Guadalajara, Jalisco, Mexico. Since 2010, he has been with the Universidad Autónoma de Ciudad Juárez, Chihuahua, Mexico, where he is currently a Professor with the Electrical and Computer Engineering Department. He has participated in various research projects in the areas of modeling and simulation of semiconductor devices and the design of digital integrated circuits and FPGAs prototyping.

MARTINS EZUMA received the B.S. degree in physics from the Federal University of Technology, Owerri, Nigeria, in 2010, the M.S. degree in information and communication engineering from Chosun University, Gwangju, South Korea, in 2015, and the M.S. degree in electrical engineering from the New Jersey Institute of Technology, in 2016. He is currently pursuing the Ph.D. degree in electrical and computer engineering with North Carolina State University, Raleigh, NC, USA. His research interests include signal processing and communications.

R. RIVERA-BLAS received the master's degree from National Polytechnic Institute, Mexico. He is currently an Associate Professor with the Master Program in Manufacture Engineering, Research and Graduate Department, ESIME-UA, Instituto Politécnico Nacional, Mexico. His research interests include robotics, image processing, and computer simulation.